Cu and Zn stable isotopes in suspended particulate matter sub-fractions from the Northern Bay of Biscay help identify biogenic and geogenic particle pools

Ferreira Araujo Daniel [1, *], Knoery Joël [1], Briant Nicolas [1], Ponzevera Emmanuel [1],
Mulholland Daniel Santos [2], Bruzac Sandrine [1], Sireau Teddy [1], Chouvelon Tiphaine [1, 2, 3],
Brach-Papa Christophe [4]

[1] Ifremer, CCEM Centre Atlantique, Unité Contamination Chimique des Écosystèmes Marins, F-44000, Nantes, France
[2] Laboratório de Águas e Efluentes & Laboratório de Análises Ambientais, Universidade Federal do Tocantins, Rua Badejos, Gurupi, TO, Brazil
[3] Observatoire Pelagis, UAR 3462 La Rochelle Université-CNRS, 17000, La Rochelle, France
[4] Ifremer, Centre Méditerranée, Unité Littoral, Laboratoire Environnement Ressources Provence-Azur-Corse (LERPAC), 83507, La Seyne-sur-Mer Cedex, France

* Corresponding author : Daniel Ferreira Araujo, email address : daniel.ferreira.araujo@ifremer.fr

Abstract :

Marine suspended particulate matter (SPM) plays a pivotal role in the marine biogeochemical cycling of trace elements. This study investigates metal distributions and copper (Cu) and zinc (Zn) stable isotope ratios in different size fractions of SPM from two sampling stations on the inner continental shelf of northern Bay of Biscay (NE Atlantic), a zone highly influenced by the macrotidal Loire estuary, the outlet of a major European river. The objective of this study is to test stable isotopes as tools to infer the origins of particles and their formation processes, and to infer relevant Cu and Zn biogenic pools involved in marine trophic transfers of these metals. SPM samples were nearly quantitatively mineralized (i.e., without HF) to determine metals and Cu and Zn isotopes in their more labile and reactive phases. Their $\delta^{65}Cu_{SRM-976}$ values ranged from −0.45 to +0.51‰, with higher Cu concentrations accompanying particle size decreasing. The $\delta^{66}Zn_{JMC-Lyon}$ values in SPM sub-fractions varied from +0.14 to +0.76‰, and were uncorrelated to both Zn concentrations and particle size. Compared to larger size fractions, increased Al and Fe levels (proxies for terrigenous materials) and enrichments in lighter Cu and Zn isotopes observed in the smaller size SPM sub-fractions suggest that a major proportion of SPM Cu and Zn is associated with geogenic particles. Conversely, the relative enrichment of heavy isotopes in coarser particles is attributable to an increase of Cu and Zn metabolically incorporated into biogenic organic particles (e.g., plankton), and by surface adsorption onto organic detrital particles. The higher δ-values attributed to biogenic particles likely represents the isotope composition of the local marine organic matter available to primary consumers like filter-feeders (oysters). Thus, this study shows that targeting particles of specific size classes allows to identify relative dominances of biogenic and geogenic carrier phases. Identifying these pools and their isotopic composition may help track Cu and Zn transfers through marine food-web metal in future studies

Graphical abstract
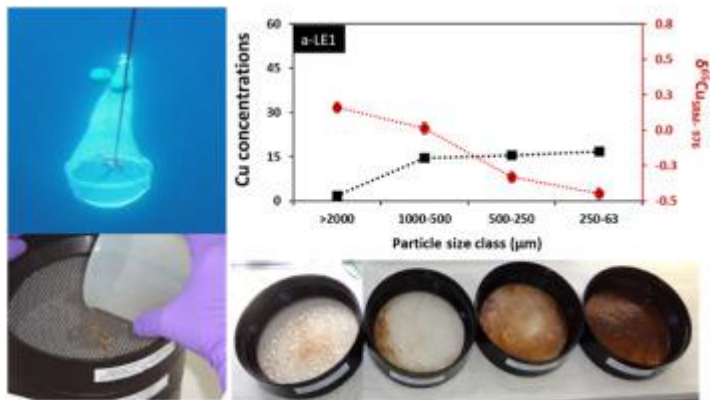
Highlights

► Cu and Zn isotopes in different particle sizes of SPM from Biscay Bay. ► Four size fractions (63–250; 250–500; 500–1000; and >2000 µm) were target. ► Isotopes help identify geogenic and biogenic pools in SPM sub-fractions. ► Geogenic pools are enriched in the light and biogenic pools in the heavy isotopes. ► Isotopes in SPM sub-fractions may help to constrain food-web metal transfers.

Keywords : Biscay Bay, Loire estuary, trace metal biogeochemistry, isotope tracer, Cu and Zn stable isotopes, MC-ICP-MS

1. Introduction

In aquatic environments, suspended particulate matter (SPM) plays a pivotal role in controlling reactivity, transport and biological uptake of trace elements (Dang, Schäfer, et al., 2015; Mason, 2013; Petit et al., 2015; Turner & Millward, 2002). It encompasses a wide range of particle sizes, from nanometers to millimeters, and includes a combination of allochthonous and autochthonous compounds of lithogenic, hydrogenic, biogenic and anthropogenic origins (Lam et al., 2018; Schulz & Zabel, 2006; Turner & Millward, 2002). It accounts for various organic compounds, including biofilms coated on clay mineral surfaces that can modify the surface texture and act as a cementing agent for sediment particles (Coutaud et al., 2014; Turner & Millward, 2002).

Trace metals can be associated with SPM as lattice structural components, or interact physico-chemically with them via adsorption, complexation, occlusion and (co)-precipitation processes (Brown & Calas, 2011; Dekov et al., 2014; Köbberich & Vance, 2018; Sparks, 2005; von der Heyden & Roychoudhury, 2015). Geochemical and biological processes (such as weathering, primary activity and hydrology) modulate interactions and distributions of trace metals in the different physicochemical SPM sub-fractions (Bianchi, 2007; de Souza Machado et al., 2016; Sparks, 2005; Tonhá et al., 2020). Therefore, their analysis in target particle classes can provide information about underlying biogeochemical processes controlling the behavior of these elements in aquatic systems, including continental shelves.

In recent years, the determination of stable copper (^{65}Cu, ^{63}Cu) and zinc (^{64}Zn, ^{66}Zn, ^{67}Zn, ^{68}Zn, ^{70}Zn) isotope abundances in environmental matrices have emerged as a new tool to examine the origins and interactions of these elements with compounds in the aquatic environment, including particles and dissolved ligands (Albarède et al., 2016; Ducher et al., 2016; Moynier et al., 2017). Heavy and light isotopes of these elements exhibit subtle differences in their chemical reactivities related to bond energies. They are unevenly distributed among reactants and products, phases, molecules, or compartments, involved in biogeochemical processes: biological uptake, redox reactions, scavenging and others (Araújo et al., 2022; Fujii et al., 2014; Little et al., 2014; Sherman & Little, 2020; Wiederhold, 2015). This isotope fractionation phenomenon occurs in a variety mechanisms and magnitudes, yielding isotope ratio changes that allow tracking Cu and Zn controlling processes (Aranda et al., 2012; Borrok et al., 2008; Skierszkan et al., 2016; Viers et al., 2018; Weiss et al., 2007).

71   In aquatic systems, the characterization of Cu and Zn isotope signatures of SPM present

72   in fluvial, lacustrine and estuarine environments has been used to trace the sources and sinks of

73   these elements (Araújo et al., 2017; Babcsányi et al., 2014; El Azzi et al., 2013; Guinoiseau et

74   al., 2018; Liang et al., 2020; Peel et al., 2009; Petit et al., 2013, 2015). However, isotope

75   description of the distribution of these elements in different size classes of aquatic SPM is

76   lacking and hence, deserves major investigations. Since particle size depends only on

77   weathering processes, biological activity and contaminant transport in the watersheds (Chester,

78   2003; Schulz & Zabel, 2006; Unda-Calvo et al., 2019), describing Cu and Zn isotope

79   compositions in the different size classes of SPM sub-fractions can provide additional

80   information about sources and processes that is not accessible when analyzing only bulk SPM.

81   For an example, in the context of Cu-contaminated soils by vineyard activity, analyses of silt

82   and fine clay fractions of the soils showed distinct Cu isotope compositions related to the

83   mineralogical and geochemical phases (Babcsányi et al., 2016; El Azzi et al., 2013). In

84   atmospheric environments, Cu and Zn isotope distribution among particle size fractions of

85   mineral dust presented a "U-shape" pattern, with lighter isotopic compositions in the mid

86   particle size fractions and heavier isotopic compositions in the smaller and larger particles

87   (Schleicher et al., 2020).

88   To date, however, very little Cu and Zn isotope data exist for particulate material from

89   the marine water column (Little et al., 2018). To fill this gap, this preliminary study examines

90   possible Cu and Zn isotope variability in different particle size classes of the SPM from the

91   northern Bay of Biscay (NE Atlantic), a local influenced by the macrotidal Loire estuary. We

92   targeted the Cu and Zn isotopes in labile, reactive and biologically available fractions of

93   particles, rather than the Cu and Zn atoms from solid lattice structures by using a "pseudo" total

94   extraction (without hydrofluoric acid). With this approach, we intend to link the observed

95   isotope patterns with biogeochemical processes, in order to constrain particle origins (inorganic

96   *vs.* organic, natural *vs.* anthropogenic) and to identify the bioorganic pools (*e.g.*, plankton) that

97   are relevant in transferring Cu and Zn to upper trophic levels. Analyses of other trace and major

98   elements are used to support the discussion.

99

100   **2. Methods**

101   *2.1 SPM sampling and preparation*

102   The Bay of Biscay is an open oceanic basin in the north-eastern Atlantic Ocean, fringed by the

103   Spanish and French coasts (Fig. 1). The continental shelf is up to about 100 miles (160 km)

104   wide off the coast of Brittany but narrows to less than 65 km off the Spanish shore. The

105   counterclockwise surface currents of the Biscay Bay are influenced by the circulation in the

106   North Atlantic. From mid-autumn to early spring (thus including winter as a whole), intense

107   river flows associated with sustained wind activity maintain this region under the influence of

108   the northward plumes of the Gironde and Loire rivers along the coast, with relatively low

109   salinities between the coast and the 100 m isobath, at around 20–40 km from the coast (Penaud

110   et al., 2020). Freshwater discharges from the main rivers (Loire, Gironde, Vilaine and Adour;

111   cumulative annual mean flow around 4200 m^3/s) in surface layers thus induce steep density

112   gradients driving a poleward circulation (about 10 cm/s) modulated by wind forcing (Lazure et

113   al., 2008; Lazure & Jegou, 1998). The climate on shore is maritime, with mild winters and cool

114   summers (Penaud et al., 2020).

115   The macrotidal Loire estuary (~106 km long) is the seaward end of Loire River, a major

116   European river, with a mean annual waterflow of 890 m^3 s^{-1}. The well mixed and highly turbid

117   sedimentary plume of this estuary extends over a large part of the northern Bay of Biscay

118   continental shelf (Dulaquais et al., 2020) (Waeles et al. 2004). The maximum turbidity zone

119   (MTZ), delimited where SPM in the water column water reach > 1g L^{-1}, is estimated to be about

120   20- to 50-km long (Briant et al., 2021; Dulaquais et al., 2020; Jalón-Rojas et al., 2016). The

121   Loire estuary has an industrialized and urbanized watershed that comprises the metropolitan

122   areas of Nantes and Saint-Nazaire with its more than 800,000 inhabitants (Grosbois et al., 2012;

123   Coynel et al., 2016).

124   A previous Cu isotope characterization of surface and core sediments in this estuary

125   indicated a dominant natural Cu origin and a spatial isotope variability related to the

126   hydrodynamic particle sorting between silt, clay, organic and amorphous particles through the

127   fluvial-estuarine continuum (Araújo et al., 2019b). In turn, Zn isotope compositions in this zone

128   was explained by natural and anthropogenic mixing source processes (Araújo et al., 2019). A

129   similar explanation was also proposed for the variations observed in oysters (*Crassostrea gigas*)

130   harvested near this estuary (Araújo et al., 2021).

131   For this study, the SPM samples near the Loire estuary were collected in April 2013 at

132   2 stations in the north Bay of Biscay inner shelf (LEP1 and LEP2). Sampling was performed

133   by successive horizontal trawls using nylon nets (0.25 m^2 circular opening, 63 μm mesh size)

134   coupled to a cylindric polymer collector at its end, in order to collect enough material in the 5

135   m below the surface for analyses. We thus considered contributions from remobilized particles

136   from bottom sediments negligible.

137   At each station, seawater samples were collected through a WP2 sampling system and

138   wet-sieved through a series of nylon sieves with mesh sizes of 2000, 1000, 500, 250 and 63 μm

139 previously cleaned with ultra-pure water in a containerized clean-room to prevent

140 contamination. A total of four sub-samples representing the following size fractions were

141 obtained for station LE1 south east of the river mouth (Fig. 1): >2000, 1000-500, 500-250, and

142 250-63 µm. The same fractions were chosen for station LE2 located north east of the river

143 mouth, except 1000-500 µm, where insufficient amounts of material were collected to allow

144 analyses. These size fractions are operationally defined and commonly used in the study of

145 trace elements in marine plankton assemblages (e.g. Chouvelon et al., 2019; Strady et al., 2015).

146 Several studies showed that size fractions >60 µm likely contain a greater fraction of (living)

147 phyto- and/or zooplankton that mostly sustain higher trophic levels, and no more detritus, viro-

148 or bacterioplankton (e.g. Rolff and Elmgren 2000, Espinasse et al. 2014).

149 Filtered seawater from the site was used to gently push SPM tangentially to the surface

150 of the sieves. Then, SPM size fractions were poured in acid-cleaned polyethylene tubes and

151 immediately frozen at -18°C. Back at the laboratory, they were freeze-dried and then stored at

152 room temperature, in the dark in the laboratory until analyses. A total between 5 and 7 g of

153 sample mass were obtained for each sampling station (Supplementary Material -Table 1S). For

154 LE1, 57% of total mass concentrated in the 63-250 µm and 16% in 250-500 µm (Table 1S). For

155 LE2, 63-250 and 250-500 µm contributed with 35 and 40% approximately. In both stations, the

156 class 500-100 µm had few materials, below 5%.

157 As noted, the SPM was collected with plankton nets and sampling protocols designed

158 to preserve as much as possible the integrity of organisms it may contain for later identification

159 and quantification (Chouvelon et al., 2019). However, these methods normally result in

160 complex samples that include both planktonic organisms and non-living organic and inorganic

161 particles. Nevertheless, this method is advantageous as it preserves cellular contents of

162 organisms and allows their concentration from tens of cubic meters of seawater. Indeed, for an

163 example, frontal-flow filtration rapidly clogs and likely induces plasmatic membrane rupture.

164 In this work, "SPM" designates the range of particle matrices present in the surface of an

165 estuarine water column and collected using a plankton net and serial wet sieving.

166

167 *2.2 Elemental and isotope analysis*

168 Dry SPM samples were weighted in Teflon® reactor vessels and digested with nitric acid

169 solution (3 ml of concentrated HNO_3 + 3 ml of H_2O) assisted by microwave radiation. This

170 method extracts metals from potentially bioavailable phases, commonly referred as water-

171 soluble, and also the exchangeable, acid-soluble, reducible, oxidable, etc. phases (Gleyzes et

172 al., 2002; Rao et al., 2008; Tessier & Turner, 1995; Tonhá et al., 2021). It is considered a partial

173   extraction of the sample, and since hydrofluoric acid (HF) that breaks down crystalline matrices

174   was not included, we consider negligible the fraction of extracted metals from crystal lattices

175   of silicates. Splits from the final solution were subsequently analyzed for metal concentrations

176   by ICP-MS (Cu, Zn, Pb, Cd, Ag, Co, Cr, Ni, Mn, Ti, V, Fe, and Al) and isotope compositions.

177   Plankton BCR 414 and oyster soft tissue SRM 1566b, as reference materials (RMs) of

178   biological matrices, were used since they are closest to the planktonic and marine characters of

179   our samples. They were processed jointly with each sample batch, including procedural blanks,

180   and recoveries are within ±10% of certified values. Similar recoveries were obtained for MESS-

181   3 reference material (RM), digested using a total extraction (e.g., with HF, as described in

182   Araújo et al., 2019a,b). The latter was used only for analytical control of isotopic analyses.

183   Cu and Zn were isolated from their matrix interferents before isotope analysis by ion

184   exchange column chromatography packed with AG-MP1 resin following an adaptation of the

185   protocol of Maréchal et al. (1999). Chromatographic recovery yields were checked by ICP-MS

186   and isotope ratios measured by MC-ICP-MS (Neptune, Thermo Scientific) at the analytical

187   platform (PSO *Pôle Spectrométrie Océan*, Ifremer, Brest, France). Samples dissolved in 2%

188   (v/v) HNO_3 medium at metal concentrations of 250 ng.ml^{-1} were introduced using a stable

189   introduction system and mass bias corrected by a combination of a sample-standard bracketing

190   combined with external normalization technique (Cu doping Zn samples and vice-versa). The

191   Cu and Zn isotope compositions of samples are expressed as $\delta^{65}Cu$ and $\delta^{66}Zn$ values, using the

192   NIST SRM 976 and the "JMC-Lyon" as reference standards according to Equations 1 and 2,

193   respectively:

194

195 $$\delta^{65}Cu_{SRM-976}\ (\text{‰}) = \left(\frac{R\left(\frac{^{65}Cu}{^{63}Cu}\right)_{sample}}{R\left(\frac{^{65}Cu}{^{63}Cu}\right)_{SRM-976}} - 1 \right) x\ 1000 \ \ (\text{Eq.1})$$

196

197 $$\delta^{66}Zn_{JMC-Lyon}\ (\text{‰}) = \left(\frac{R\left(\frac{^{66}Zn}{^{64}Zn}\right)_{sample}}{R\left(\frac{^{66}Zn}{^{64}Zn}\right)_{JMC-Lyon}} - 1 \right) x\ 1000 \ \ (\text{Eq. 2})$$

198

199   The average precision (2s) obtained from two or three measurements for a single replicate

200   during a unique analytical session was ±0.04‰ for both analytes. Our obtained $\delta^{65}Cu_{SRM-976}$

201   value for the plankton RM BCR 414 (-0.27 ± 0.02‰, 2s, *n* = 3) agreed with reported values in

202 literature (-0.29 ± 0.10‰, 2σ, $n = 3$, Yang et al., 2020; -0.27 $\pm$ 0.05‰, Takano et al., 2020),

203 while the corresponding $\delta^{66}Zn_{JMC}$ for this RM (+0.23 $\pm$0.09‰, 2s, $n = 1$) fell in the same range

204 of values reported by Takano et al.(2020) of +0.31 $\pm$ 0.03‰ (2s, $n = 10$). Longer time series of

205 analyses of the oyster tissue SRM 1566b yielded reproductible $\delta^{65}Cu_{SRM-976}$ and $\delta^{66}Zn_{JMC}$ values

206 of +0.23 $\pm$0.03‰ (2s, $n = 11$) and +0.70 $\pm$0.05‰ (2s, $n = 5$), respectively. These values are

207 close to the $\delta^{65}Cu_{SRM-976}$ value of +0.30 $\pm$0.02 (2s, $n=4$, Jeong et al., 2021) and $\delta^{66}Zn_{JMC}$ values

208 of +0.68 $\pm$ 0.04‰ ($n= 14$, 2s, Nitzsche et al., 2021). Measurements of the sediment MESS-3

209 RM during several analytical sessions yielded a $\delta^{66}Zn_{JMC}$ of +0.26 $\pm$ 0.06‰ (2s, $n= 9$), which

210 agrees with another published value (+0.28 $\pm$ 0.02‰ , 2s, $n= 4$, Druce et al., 2020). The

211 corresponding $\delta^{65}Cu_{SRM-976}$ for this sediment was +0.03 $\pm$0.1 ($n= 9$), but no literature data are

212 available for comparison.

213

214 *2.3 Principal Component Analysis (PCA)*

215 Principal Component Analysis (PCA) was applied to identify the main interrelations among the

216 elemental variables, and hence, summarizing dataset information by grouping inter-correlated

217 variables in principal components (Meglen, 1992). PCA factor loads were calculated using the

218 correlation matrix with varimax rotation. The principal components (PCs) that had eigenvalues

219 higher than 1 were selected for discussion (Mar da Costa et al., 2016; Mulholland et al., 2012).

220 The communalities values of all variables equal or higher than 0.5 were used as thresholds for

221 PCA results acceptance (Araújo, et al., 2019). PCA analysis was performed using the SPSS®

222 software v.18.0 (IBM®). Linear relationship between variables were estimated using Pearson

223 coefficients.

224

225 **3. Results and discussion**

226

227 *3.1 Elemental and isotope distributions in the SPM sub-fractions*

228 Concentrations of Cu vary from 2 to 57 µg g^{-1} dry weight (dw) and display an overall tendency

229 of increasing with decreasing particle size (Table 1; Fig. 2a,b). In turn, Zn concentrations range

230 from 66 to 200 µg g^{-1} dw and are uncorrelated with particle size, with the highest Zn

231 concentrations observed in intermediate-size fractions (Table 1; Fig. 2c,d). The $\delta^{65}Cu_{SRM-976}$

232 values of both sampling stations range from -0.45 to +0.51‰, while $\delta^{66}Zn_{JMC}$ values vary from

233 +0.14 to +0.76‰. For both sites, the elemental and isotope Cu systematics demonstrate a clear

234 trend towards lighter Cu isotope compositions and higher concentrations with smaller particle

235 sizes (Fig. 2a,b). Zinc stable isotope systematics are less clear (Fig. 2c,d), even if the lightest

236 isotope compositions occur in the smallest size class 63-250 µm that was collected at both

237 sampling stations, and in the 250-500 µm class of the LE2 sample. A comparison of particle

238 classes of the same sizes shows similar values at both sites, except for Zn in the class size 250-

239 500 µm.

240   Principal Component Analysis (PCA) was applied to the dataset to visualize the

241 intercorrelations between the concentrations of Cu and Zn and other elements. It yields two

242 main components that together explained 92% of total dataset variance and discriminated two

243 clusters of elements, here labelled as "Group A" and "Group B", respectively (Fig. 3a). Group

244 A comprises Cu, Pb, Ni, Cr, Co, Mn, V, Ti, Al and Fe, while Group B includes Zn, Cd, and Ag

245 (Fig. 3a). Elements from the first cluster show an overall tendency of concentration increase

246 with particle size decrease, analogous to Cu (Table 1). In the second cluster, the elements

247 display highest concentrations in intermediate size fractions, similarly to Zn (Table 1). In Group

248 A, major elements (Al and Fe) and trace elements (Mn, V, Ti, Co, Cr, V, Pb, and Ni) showed

249 strong coefficients of correlations ($r > 0.9$, $p < 0.01$), while in Group B, Cd and Ag are strongly

250 correlated among them ($r > 0.9$, $p < 0.01$). Copper show affinities with Cr and Ni ($0.7 < r < 0.9$,

251 $p < 0.05$). In turn, Zn is not significantly correlated to Cd and Ag ($0.1 < p > 0.05$), despite

252 belonging in the same cluster.

253   In the southernmost LE1 sampling station, the finer SPM sub-fraction of 63-250 µm

254 contribute with 73% of total Cu mass. Based on the mass sub-fractions and their respective Cu

255 concentrations we estimate a bulk SPM concentration of 13 µg g^{-1} and a δ^{65}Cu value near -

256 0.27‰ (Table 1S). This estimated isotope value is much lighter than the average obtained for

257 the bottom sediments from the Loire estuary mouth and its vicinities (-0.04 ± 0.18, 2s, n=31,

258 Araújo et al., 2019b). For Zn, estimations yield a concentration of 96 µg g^{-1} and a δ^{66}Zn value

259 of +0.43‰, which fell above the average of the local sedimentary surface ($+0.24 \pm 0.06$, 2s,

260 n=25). The difference between bulk SPM and bottom sediments suggest differences in their

261 physicochemical compositions of each compartment. Surface sediments tend to be enriched in

262 denser particles that settled through the water-column and their composition modified by early

263 diagenesis occurring immediately below.(Coynel et al., 2016; Dang, et al., 2015). An

264 unfortunately missing analysis of the (1000-500 µm) fractions did not allow to estimate bulk

265 values at LE2.

266

267 *3.2 Using Cu isotope information to infer particle origins and underlying processes*

268 The northern continental shelf Bay of Biscay receives high loads of metals associated with i)

269 inorganic and organic particles derived from weathering and erosion of the continental surface,

270 ii) in situ primary productivity, and iii) anthropogenic emissions from the Loire estuary

271 watershed (Araújo, et al., 2019b; Briant et al., 2017, 2021; Coynel et al., 2016; Penaud et al.,

272 2020). This particulate material is likely the main source of the elements from group "A" in the

273 PCA analysis (Cu, Al, Fe, Mn, V, Cr, Ni, Ti, Pb, Co). The similar Fe to Al ratio in all the SPM

274 samples indicates that the relative proportions of these two major elements are constant across

275 the different particle size classes (Fig. 3b), which demonstrates that terrigenous materials are

276 ubiquitous in the samples. Figure 3b also shows that, increased Fe and Al concentrations with

277 decreasing particle size indicates a stronger imprint of "continental" inorganic (i.e., Fe and Al-

278 containing) particles on the smaller size class particles (Fig. 3b). The accompanying

279 concentration of the "continental" trace elements (group "A"), including Cu, point to the role

280 of geogenic particles, mostly composed of clay minerals and their surface coatings, in

281 transporting these elements from estuary mouth to the shelf of the bay.

282   The observed lighter Cu isotope compositions of finer particles are also consistent with

283 the presence of weathered, smaller-size minerals and their increased capacity to adsorb this

284 trace metal. In the critical zone, once released from their primary mineral structures, Cu isotopes

285 tend to partition between aqueous organic complexes and residual particulate phases (Fe-Mn

286 oxyhydroxides, clay minerals). The former become enriched with the heavy isotopes, while the

287 latter become enriched with the light isotopes (Little et al., 2014; Vance et al., 2016). Field

288 studies observed the link between enrichment of light isotopes in clay minerals with primary

289 mineral depletion in soils (Guinoiseau et al., 2017, 2018b), while batch experiments showed

290 the preferential light isotope adsorption on the surface of kaolinite (Li et al., 2015), and

291 preferential heavy isotope losses in acid-leachates on natural basalts (Li & Liu, 2022). The

292 coherence of our results with the cited field and laboratory studies point to weathering as the

293 primary source of Cu with cumulative effects of organic ligands adsorption on solid surfaces as

294 the principal controlling processes of group "A" (continental) elements in the finer particle size

295 classes.

296   Conversely, the coarser SPM fractions exhibit lower concentration of crustal elements

297 (Table 1), and hence, we infer that the relative fraction of organic matter, which includes living

298 organisms and detrital forms of plants and micro-organisms, should increase. It is well known

299 that Cu presents high affinity with organic matter (Ilina et al., 2013). Furthermore, experimental

300 adsorption of Cu isotopes on organic matter (insolubilized humic acid-IHA) indicates the

301 preferential retention of the heavy isotope in the organo-Cu complexes (Bigalke et al., 2010).

302 Similarly, Cu adsorption onto phototrophic biofilm induces enrichment of biomass in heavy

303 isotope (Coutaud et al., 2014). These observations suggest that Cu-organic matter-associations

304   in the SPM fractions could form a pool of isotopically heavy Cu. Indeed, the homeostatic
305   regulation of Cu in microorganisms, such as in meso- and macro-plankton could result in an
306   isotopically heavy, bioaccumulated Cu pool. It is well-know that Cu heavy isotopes
307   preferentially tend to bound to O- and N- donors of proteins involved in metabolic functions
308   (Albarède et al., 2016). Conversely, light Cu isotopes would be preferentially associated to S-
309   ligands often used for detoxification and excretion processes. High positive $\delta^{65}Cu$ values found
310   in sheep and mouse kidney has been also interpreted in terms of isotope fractionation in redox
311   reactions involving Cu (I) and Cu (II) species. These dual and opposite effects fractionation
312   mechanisms were also used to explain Cu isotope systematic observed in mussels (Araújo, et
313   al., 2021). It is unknown if the plankton of distinct size classes, composed of different species
314   assemblages present different isotope enrichment patterns related to metabolic and homeostatic
315   processes. In any case, the Cu isotope systematic presented here identifies two main Cu pools
316   in suspended particulate matter: a mineral rich (continental) pool, enriched in light isotopes,
317   and an organic-rich, labile pool, enriched in the heavy isotope. Such a systematic is very similar
318   to the particulate phase of South Atlantic ocean waters (Little et al., 2018).

319

320   *3.3 Using Zn isotope composition to infer particle origins and underlying processes*

321   The inter-correlations among Cd, Zn, and Ag identified in PCA analysis suggest that these
322   elements are less influenced by the detrital, terrigenous materials that are preferentially present
323   in the smaller-size SPM sub-fractions. Their concentrations and mass contents do not increase
324   with decreasing particulate size. Rather, they tend to be highest in intermediate size fractions
325   of SPM (Fig. 2c,d, for Zn; Table 1, for Ag and Cd). A similar pattern was also reported, but not
326   explained, in another study conducted in Gulf of Lions (NW Mediterranean Sea, Chouvelon et
327   al., 2019) using an analogous sample preparation, that is, seawater passed through sieves of
328   decreasing mesh (200, 60 and 6 µm). The authors related the observed Cd, Zn and Ag
329   distributions in SPM sub-fractions to the assimilation of Zn, Cd and Ag by copepods via
330   protozoa diet (Chouvelon et al., 2019), despite the lack of detailed information about actual
331   species distribution in the various SPM fractions. Indeed, the literature shows biomagnification
332   of Zn, Cd and Ag in the low part of the trophic chain (Reinfelder et al. 1998). A higher Zn
333   association with biologically-influenced particles is consistent with its status as the second-
334   most abundant micronutrient in phytoplankton biomass (Morel, 2003; Twining & Baines,
335   2013).

336   The smallest size-classes of the SPM in LE1 (250-63 µm) and LE2 (500-250 µm and
337   250-63 and) displayed $\delta^{66}Zn$ values within the range for Loire estuary bottom sediments, about

338 +0.24 ± 0.11 (2s, *n*=26, Araújo et al., 2019). Zinc concentration of the surface sediment in the

339 Loire estuary mouth is influenced by geogenic ($\delta^{66}Zn_{JMC}$ ~0.3‰) and anthropogenic Zn

340 ($\delta^{66}Zn_{JMC}$ ~0.1‰). Thus, these natural and anthropic Zn sources may also be reflected in the

341 Zn isotope compositions observed in the finer particle fractions of LE1 and LE2 sampling

342 stations.

343   Overall, Zn isotope variability of smaller, geogenic particles is close to crustal rocks

344 since isotope fractionation along weathering processes is small, but a subtle isotope

345 fractionation with preferential allocation of the heavy and light isotope in particulate and

346 dissolved phases is noticeable in most field samples (Desaulty & Petelet-Giraud, 2020;

347 Guinoiseau et al., 2018b; Little et al., 2014; Moynier et al., 2017; Suhr et al., 2018; Vance et

348 al., 2016). Like for Cu, geogenic Zn isotope signatures seems to result from the balance between

349 complexation by organic ligands and sorption on solid surfaces in weathering processes.

350   It is important to note that, like models, laboratory work does not include the complexity

351 and conditions of real systems, which may yield findings different than field observations. For

352 example, Zn batch adsorption experiments have mostly demonstrated a preferential binding of

353 the heavy isotope in surfaces of clay minerals and Fe-Mn-Al oxyhydroxides (Komárek et al.,

354 2021). However, in estuaries (e.g., Gironde and Pearl Harbor), it has observed an unexpected

355 preferential removal of the light Zn isotope from the dissolved fraction via sorption processes

356 on surface particles through the maximum turbidity zones (Ma et al., 2020; Petit et al., 2015).

357 The mismatch between field and laboratory results can also be related to equilibrium conditions

358 built into experimental designs, whereas natural processes in dynamic areas close estuaries can

359 occur kinetically-driven.

360   Anthropogenic Zn from urban and industrial emissions, mainly released by the erosion

361 of Zn-plated materials, vehicular traffic (tires and brake pad wear, and combustion), and sewage

362 has lighter isotope values centered around 0.1‰ (Desaulty & Petelet-Giraud, 2020; Nitzsche et

363 al., 2021; Thapalia et al., 2015). Urban and industrial agglomerations close to estuaries

364 represent several anthropogenic sources, and thus multi Zn emissions should occurs almost

365 concomitantly (Barletta et al., 2019; Burt et al., 2019; Desaulty & Petelet-Giraud, 2020). Their

366 mixing along the fluvial-estuarine continuum and in continental run-off makes pinpointing

367 specific Zn sources challenging, generally requiring the combination of additional elemental

368 and isotope source proxies (Gonzalez et al., 2016; Souto-Oliveira et al., 2019). Here, $\delta^{66}Zn$

369 values has been proved a good proxy to detect "Zn urban fingerprints" in the coastal

370 environments (Zhang et al., 2018).

371   Nonetheless, the source mixing processes involving anthropogenic and geogenic Zn do
372   not explain the heavier isotope enrichments (above 0.6‰) in the coarser fractions (> 250 µm in
373   LE1 and > 500 µm in LE2). Such as inferred for Cu, a relative increase of a Zn-rich organic
374   pool in the SPM coarser fractions should occur along with a decrease in the geogenic pool.
375   Indeed, zinc associates with organic matter via physico-chemical reactions with organic solid
376   surfaces of humic and fulvic acids, and with cell walls of living organisms, or with detrital
377   material resulting of microbial degradation of plant or animal (Brown & Calas, 2011). Previous
378   studies have argued that the scavenging of Zn from a marine water column onto organic particle
379   surfaces favors the retention of heavier Zn isotopes in the particulate phase (Gélabert et al.,
380   2006; John & Conway, 2014; Weber et al., 2018). This is coherent with the observed δ^{66}Zn
381   distributions in vertical seawater profiles from the Atlantic and Pacific oceans (John et al.,
382   2018). The isotope distribution pattern resulting from this open ocean process also seems to
383   hold true for our study site on the continental shelf. There, in parallel to physico-chemical
384   sorption processes, intracellular uptake of Zn can also occur favoring the light isotope
385   enrichment in living cells via kinetically-driven isotope fractionation (Twining & Baines, 2013;
386   Araújo et al., 2018; Caldelas et al., 2011; John et al., 2007; Köbberich & Vance, 2019).
387   However, given the relatively high δ^{66}Zn values from biogenic particles, the hypothesis of
388   cellular uptake seems to be a minor influence on the Zn isotope compositions in the studied
389   sub-fractions.

390

391   *3.4 Isotope identification of biogenic pools and their relevance for marine trophic web studies*
392   For our samples, the previous sections suggested that biogenic pools predominate in coarser
393   sub-fractions and have heavier isotope compositions than geogenic ones. Indeed, for Zn, as the
394   biogenic pool increases in larger sized SPM sub-fractions, δ^{66}Zn values increase, approaching
395   that of local filter-feeding organisms (oysters) (Fig. 4). The nearing SPM and biota isotope
396   signatures suggest that the "biogenic Zn" pool from SPM is available for bioaccumulation in
397   upper trophic levels via dietary intake, and therefore, does represent the local marine trophic
398   baseline. Below are the main arguments in support of our suggestion that δ^{66}Zn isotope values
399   in oysters are consistent with the hypothesis of a bioavailable biogenic Zn pool.

400   Oysters are filter-feeders capable of filtering large quantities of seawater to extract their
401   sustenance from seston (e.g., phytoplankton and algae debris). (Dame, 2012; Gosling, 2003;
402   Wang and Wang, 2019). Being primary consumers, the isotope composition of carbon and
403   nitrogen in their tissues are reliable proxies to assess their organic dietary sources (Briant et al.,
404   2018). Furthermore, they accumulate metals through both particulate and dissolved pathways.

405 The particulate phase is associated with the diet and is considered the main route of
406 bioaccumulation (Akcha et al., 2022; Griscom & Fisher, 2004). Oysters' ability to uptake
407 contaminants and especially metals in their tissues justifies their wide use for biomonitoring
408 marine environments. Recently, determinations of metal isotopes in oysters from biomonitoring
409 sample banks has inferred anthropogenic origins and bioaccumulation routes for these
410 elements. Since internal biological Zn fractionation of oysters does not affect the isotope record
411 of Zn sources, these organisms are a reliable proxy of the Zn to which they are exposed in the
412 surrounding medium (Ma et al., 2019; Ma & Wang, 2021). Therefore, Zn isotopes in the
413 temporal series of bivalves have helped reconstruct anthropogenic Zn bioaccumulation
414 tendencies in French estuaries (Araújo, et al., 2021).

415 Furthermore, in a spatial sampling of these organisms paired with SPM and water
416 samples from the Pearl Harbor estuary, (Ma et al., 2021) quantified relative fractions of Zn
417 bioaccumulated via dissolved and particulate routes, assuming that Zn from bulk SPM was
418 entirely bioavailable. This assumption, however, is not necessarily true in natural systems and
419 it may be necessary to refine uptake models for quantifying relative fractions contributions
420 more accurately. Indeed, selective extractions using organic solvents (e.g., isopropanol) in
421 continental margin sediments worldwide revealed that soluble organic fractions have heavier
422 Zn isotope compositions (>0.5‰ than the bulk material (~0.3‰) analyzed (Y. Zhang et al.,
423 2021). Like our samples, the prevalent heavy isotope in these organic factions has also been
424 associated with biological activity and scavenging processes. Interestingly, the heavy isotope
425 enrichment in biogenic materials seems coherent with organic-derived materials, such as
426 bituminous coal (~1.3‰, Gonzalez & Weiss, 2015). With oyster isotope records as a proxy of
427 bioavailable Zn, the all mentioned evidence supports our hypothesis that a biogenic pool
428 enriched in the heavy isotope is a primary Zn source for these organisms.

429

430 **4. Conclusions**

431 This study reports for the first-time the isotope compositions of Cu and Zn in different size
432 fractions of SPM (63-250; 250-500; 500-1000; and 1000-2000 µm) from a continental shelf.
433 These data showed significant isotope variability between particle size fractions greater than
434 that observed for bulk bottom sediment collected over the entire study site (e.g., for Zn, Fig. 4).
435 The Cu and Zn isotope systematics, combined with the elemental composition dataset, allowed
436 to distinguish two main Cu and Zn pools within the SPM. These pools control the behavior of
437 these elements: the (relatively) refractory geogenic pool is enriched in light isotopes, while the
438 (relatively) labile pool is enriched in heavy isotopes. Both pools are present in all SPM sub-

439 fractions, but their relative proportions vary according to particle size. The observed heavier
440 isotope composition of biogenic particles likely reflects the local trophic marine baseline and
441 explains the close isotope values observed in secondary consumers (i.e., oysters). We suggest
442 that combining target-specific size classes and using selective extractions may improve the
443 isotope characterization of different metal pools which may have different bioavailabilities. For
444 bivalves, isotope characterization of metals in particles from the size range of food particles (1-
445 10 µm, Gosling, 2003) is suggested, to enable source apportionment of bioaccumulation routes
446 (dissolved *vs*. particulate).

447 This study confirms that isotope analyses in distinct class-sized particles can provide
448 additional information related to host phases of Cu and Zn, and their entry at the base of the
449 trophic food-web. For future studies on trace metals, we recommend combining mineralogical
450 and plankton assemblages with speciation and isotope characterization. This information will
451 allow to better understand the influence of particle composition on the input, dissolution,
452 scavenging, (dis-)aggregation, and transport of these elements in the marine environment.

453

454 **Acknowledgements**

459 **References**

460 Akcha, F., Coquillé, N., Sussarellu, R., Rouxel, J., Chouvelon, T., Gonzalez, P., Legeay, A., Bruzac,
461   S., Sireau, T., Gonzalez, J.-L., Gourves, P.-Y., Godfrin, Y., Buchet, V., & Stachowski-
462   Haberkorn, S. (2022). Trophic transfer of copper decreases the condition index in Crassostrea
463   gigas spat in concomitance with a change in the microalgal fatty acid profile and enhanced
464   oyster energy demand. *Science of The Total Environment*, *824*, 153841.
465   https://doi.org/10.1016/j.scitotenv.2022.153841
466 Albarede, F., Télouk, P., Balter, V., Bondanese, V. P., Albalat, E., Oger, P., Bonaventura, P., Miossec,
467   P., & Fujii, T. (2016). Medical applications of Cu, Zn, and S isotope effects. *Metallomics*,
468   *8*(10), 1056–1070. https://doi.org/10.1039/C5MT00316D
469 Aranda, S., Borrok, D. M., Wanty, R. B., & Balistrieri, L. S. (2012). Zinc isotope investigation of
470   surface and pore waters in a mountain watershed impacted by acid rock drainage. *Science of
471   The Total Environment*, *420*, 202–213. https://doi.org/10.1016/j.scitotenv.2012.01.015
472 Araújo, D. F., Knoery, J., Briant, N., Vigier, N., & Ponzevera, E. (2022). "Non-traditional" stable
473   isotopes applied to the study of trace metal contaminants in anthropized marine environments.
474   *Marine Pollution Bulletin*, *175*, 113398. https://doi.org/10.1016/j.marpolbul.2022.113398
475 Araújo, D. F., Machado, W., Weiss, D., Mulholland, D. S., Garnier, J., Souto-Oliveira, C. E., &
476   Babinski, M. (2018). Zinc isotopes as tracers of anthropogenic sources and biogeochemical
477   processes in contaminated mangroves. *Applied Geochemistry*, *95*, 25–32.
478   https://doi.org/10.1016/j.apgeochem.2018.05.008
479 Araújo, D. F., Ponzevera, E., Briant, N., Knoery, J., Bruzac, S., Sireau, T., & Brach-Papa, C. (2019).
480   Copper, zinc and lead isotope signatures of sediments from a mediterranean coastal bay

481   impacted by naval activities and urban sources. *Applied Geochemistry*, *111*, 104440.
482   https://doi.org/10.1016/j.apgeochem.2019.104440

483   Araújo, D. F., Ponzevera, E., Briant, N., Knoery, J., Bruzac, S., Sireau, T., Pellouin-Grouhel, A., &
484   Brach-Papa, C. (2021). Differences in Copper Isotope Fractionation Between Mussels
485   (Regulators) and Oysters (Hyperaccumulators): Insights from a Ten-Year Biomonitoring
486   Study. *Environmental Science & Technology*, *55*(1), 324–330.
487   https://doi.org/10.1021/acs.est.0c04691

488   Araújo, D. F., Ponzevera, E., Briant, N., Knoery, J., Sireau, T., Mojtahid, M., Metzger, E., & Brach-
489   Papa, C. (2019). Assessment of the metal contamination evolution in the Loire estuary using
490   Cu and Zn stable isotopes and geochemical data in sediments. *Marine Pollution Bulletin*, *143*,
491   12–23. https://doi.org/10.1016/j.marpolbul.2019.04.034

492   Araújo, D. F., Ponzevera, E., Weiss, D. J., Knoery, J., Briant, N., Yepez, S., Bruzac, S., Sireau, T., &
493   Brach-Papa, C. (2021). Application of Zn Isotope Compositions in Oysters to Monitor and
494   Quantify Anthropogenic Zn Bioaccumulation in Marine Environments over Four Decades: A
495   "Mussel Watch Program" Upgrade. *ACS ES&T Water*, *1*(4), 1035–1046.
496   https://doi.org/10.1021/acsestwater.1c00010

497   Araújo, D., Machado, W., Weiss, D., Mulholland, D. S., Boaventura, G. R., Viers, J., Garnier, J.,
498   Dantas, E. L., & Babinski, M. (2017). A critical examination of the possible application of
499   zinc stable isotope ratios in bivalve mollusks and suspended particulate matter to trace zinc
500   pollution in a tropical estuary. *Environmental Pollution*, *226*, 41–47.
501   https://doi.org/10.1016/j.envpol.2017.04.011

502   Babcsányi, I., Chabaux, F., Granet, M., Meite, F., Payraudeau, S., Duplay, J., & Imfeld, G. (2016).
503   Copper in soil fractions and runoff in a vineyard catchment: Insights from copper stable
504   isotopes. *Science of The Total Environment*, *557–558*, 154–162.
505   https://doi.org/10.1016/j.scitotenv.2016.03.037

506   Babcsányi, I., Imfeld, G., Granet, M., & Chabaux, F. (2014). Copper Stable Isotopes To Trace Copper
507   Behavior in Wetland Systems. *Environmental Science & Technology*, *48*(10), 5520–5529.
508   https://doi.org/10.1021/es405688v

509   Barletta, M., Lima, A. R. A., & Costa, M. F. (2019). Distribution, sources and consequences of
510   nutrients, persistent organic pollutants, metals and microplastics in South American estuaries.
511   *Science of The Total Environment*, *651*, 1199–1218.
512   https://doi.org/10.1016/j.scitotenv.2018.09.276

513   Bianchi, T. S. (2007). *Biogeochemistry of estuaries*. Oxford University Press.

514   Bigalke, M., Weyer, S., & Wilcke, W. (2010). Copper Isotope Fractionation during Complexation
515   with Insolubilized Humic Acid. *Environmental Science & Technology*, *44*(14), 5496–5502.
516   https://doi.org/10.1021/es1017653

517   Borrok, D. M., Nimick, D. A., Wanty, R. B., & Ridley, W. I. (2008). Isotopic variations of dissolved
518   copper and zinc in stream waters affected by historical mining. *Geochimica et Cosmochimica*
519   *Acta*, *72*(2), 329–344. https://doi.org/10.1016/j.gca.2007.11.014

520   Briant, N., Chiffoleau, J.-F., Knoery, J., Araújo, D. F., Ponzevera, E., Crochet, S., Thomas, B., &
521   Brach-Papa, C. (2021). Seasonal trace metal distribution, partition and fluxes in the temperate
522   macrotidal Loire Estuary (France). *Estuarine, Coastal and Shelf Science*, *262*, 107616.
523   https://doi.org/10.1016/j.ecss.2021.107616

524   Briant, N., Chouvelon, T., Martinez, L., Brach-Papa, C., Chiffoleau, J., Savoye, N., Sonke, J., &
525   Knoery, J. (2017). Spatial and temporal distribution of mercury and methylmercury in
526   bivalves from the French coastline. *Marine Pollution Bulletin*, *114*(2), 1096–1102.
527   https://doi.org/10.1016/j.marpolbul.2016.10.018

528   Brown, G. E., & Calas, G. (2011). Environmental mineralogy – Understanding element behavior in
529   ecosystems. *Comptes Rendus Geoscience*, *343*(2), 90–112.
530   https://doi.org/10.1016/j.crte.2010.12.005

531   Burt, J. A., Killilea, M. E., & Ciprut, S. (2019). Coastal urbanization and environmental change:
532   Opportunities for collaborative education across a global network university. *Regional Studies*
533   *in Marine Science*, *26*, 100501. https://doi.org/10.1016/j.rsma.2019.100501

534   Caldelas, C., Dong, S., Araus, J. L., & Jakob Weiss, D. (2011). Zinc isotopic fractionation in
535   Phragmites australis in response to toxic levels of zinc. *Journal of Experimental Botany*,
536   *62*(6), 2169–2178. https://doi.org/10.1093/jxb/erq414

537   Chester, R. (2003). *Marine geochemistry* (2. ed). Blackwell Science.

538   Chouvelon, T., Strady, E., Harmelin-Vivien, M., Radakovitch, O., Brach-Papa, C., Crochet, S.,
539   Knoery, J., Rozuel, E., Thomas, B., Tronczynski, J., & Chiffoleau, J.-F. (2019). Patterns of
540   trace metal bioaccumulation and trophic transfer in a phytoplankton-zooplankton-small
541   pelagic fish marine food web. *Marine Pollution Bulletin*, *146*, 1013–1030.
542   https://doi.org/10.1016/j.marpolbul.2019.07.047

543   Coutaud, A., Meheut, M., Viers, J., Rols, J.-L., & Pokrovsky, O. S. (2014). Zn isotope fractionation
544   during interaction with phototrophic biofilm. *Chemical Geology*, *390*, 46–60.
545   https://doi.org/10.1016/j.chemgeo.2014.10.004

546   Coynel, A., Gorse, L., Curti, C., Schafer, J., Grosbois, C., Morelli, G., Ducassou, E., Blanc, G.,
547   Maillet, G. M., & Mojtahid, M. (2016). Spatial distribution of trace elements in the surface
548   sediments of a major European estuary (Loire Estuary, France): Source identification and
549   evaluation of anthropogenic contribution. *Journal of Sea Research*, *118*, 77–91.
550   https://doi.org/10.1016/j.seares.2016.08.005

551   Dang, D. H., Lenoble, V., Durrieu, G., Omanović, D., Mullot, J.-U., Mounier, S., & Garnier, C.
552   (2015). Seasonal variations of coastal sedimentary trace metals cycling: Insight on the effect
553   of manganese and iron (oxy)hydroxides, sulphide and organic matter. *Marine Pollution*
554   *Bulletin*, *92*(1–2), 113–124. https://doi.org/10.1016/j.marpolbul.2014.12.048

555   Dang, D. H., Schäfer, J., Brach-Papa, C., Lenoble, V., Durrieu, G., Dutruch, L., Chiffoleau, J.-F.,
556   Gonzalez, J.-L., Blanc, G., Mullot, J.-U., Mounier, S., & Garnier, C. (2015). Evidencing the
557   Impact of Coastal Contaminated Sediments on Mussels Through Pb Stable Isotopes
558   Composition. *Environmental Science & Technology*, *49*(19), 11438–11448.
559   https://doi.org/10.1021/acs.est.5b01893

560   de Souza Machado, A. A., Spencer, K., Kloas, W., Toffolon, M., & Zarfl, C. (2016). Metal fate and
561   effects in estuaries: A review and conceptual model for better understanding of toxicity.
562   *Science of The Total Environment*, *541*, 268–281.
563   https://doi.org/10.1016/j.scitotenv.2015.09.045

564   Dekov, V. M., Vanlierde, E., Billström, K., Garbe-Schönberg, C.-D., Weiss, D. J., Gatto Rotondo, G.,
565   Van Meel, K., Kuzmann, E., Fortin, D., Darchuk, L., & Van Grieken, R. (2014). Ferrihydrite
566   precipitation in groundwater-fed river systems (Nete and Demer river basins, Belgium):
567   Insights from a combined Fe-Zn-Sr-Nd-Pb-isotope study. *Chemical Geology*, *386*, 1–15.
568   https://doi.org/10.1016/j.chemgeo.2014.07.023

569   Desaulty, A.-M., & Petelet-Giraud, E. (2020). Zinc isotope composition as a tool for tracing sources
570   and fate of metal contaminants in rivers. *Science of The Total Environment*, *728*, 138599.
571   https://doi.org/10.1016/j.scitotenv.2020.138599

572   Druce, M., Stirling, C. H., & Rolison, J. M. (2020). High-Precision Zinc Isotopic Measurement of
573   Certified Reference Materials Relevant to the Environmental, Earth, Planetary and Biomedical
574   Sciences. *Geostandards and Geoanalytical Research*, *44*(4), 711–732.
575   https://doi.org/10.1111/ggr.12341

576   Ducher, M., Blanchard, M., & Balan, E. (2016). Equilibrium zinc isotope fractionation in Zn-bearing
577   minerals from first-principles calculations. *Chemical Geology*, *443*, 87–96.
578   https://doi.org/10.1016/j.chemgeo.2016.09.016

579   Dulaquais, G., Waeles, M., Breitenstein, J., Knoery, J., & Riso, R. (2020). Links between size
580   fractionation, chemical speciation of dissolved copper and chemical speciation of dissolved
581   organic matter in the Loire estuary. *Environmental Chemistry*, *17*(5), 385.
582   https://doi.org/10.1071/EN19137

583   El Azzi, D., Viers, J., Guiresse, M., Probst, A., Aubert, D., Caparros, J., Charles, F., Guizien, K., &
584   Probst, J. L. (2013). Origin and fate of copper in a small Mediterranean vineyard catchment:
585   New insights from combined chemical extraction and δ65Cu isotopic composition. *Science of*
586   *The Total Environment*, *463–464*, 91–101. https://doi.org/10.1016/j.scitotenv.2013.05.058

587   Fujii, T., Moynier, F., Blichert-Toft, J., & Albarède, F. (2014). Density functional theory estimation of
588   isotope fractionation of Fe, Ni, Cu, and Zn among species relevant to geochemical and
589   biological environments. *Geochimica et Cosmochimica Acta*, *140*, 553–576.
590   https://doi.org/10.1016/j.gca.2014.05.051

591   Gélabert, A., Pokrovsky, O. S., Viers, J., Schott, J., Boudou, A., & Feurtet-Mazel, A. (2006).
592   Interaction between zinc and freshwater and marine diatom species: Surface complexation and

593   Zn isotope fractionation. *Geochimica et Cosmochimica Acta*, *70*(4), 839–857.
594   https://doi.org/10.1016/j.gca.2005.10.026

595 Gleyzes, C., Tellier, S., & Astruc, M. (2002). Fractionation studies of trace elements in contaminated
596   soils and sediments: A review of sequential extraction procedures. *TrAC Trends in Analytical*
597   *Chemistry*, *21*(6), 451–467. https://doi.org/10.1016/S0165-9936(02)00603-9

598 Gonzalez, R. O., Strekopytov, S., Amato, F., Querol, X., Reche, C., & Weiss, D. (2016). New Insights
599   from Zinc and Copper Isotopic Compositions into the Sources of Atmospheric Particulate
600   Matter from Two Major European Cities. *Environmental Science & Technology*, *50*(18),
601   9816–9824. https://doi.org/10.1021/acs.est.6b00863

602 Gonzalez, R., & Weiss, D. (2015). Zinc Isotope Variability in Three Coal-Fired Power Plants: A
603   Predictive Model for Determining Isotopic Fractionation during Combustion. *Environmental*
604   *Science & Technology*, *49*(20), 12560–12567. https://doi.org/10.1021/acs.est.5b02402

605 Gosling, E. M. (2003). *Bivalve molluscs: Biology, ecology, and culture*. Fishing News Books.

606 Griscom, S. B., & Fisher, N. S. (2004). Bioavailability of sediment-bound metals to marine bivalve
607   molluscs: An overview. *Estuaries*, *27*(5), 826–838. https://doi.org/10.1007/BF02912044

608 Guinoiseau, D., Bouchez, J., Gélabert, A., Louvat, P., Moreira-Turcq, P., Filizola, N., & Benedetti, M.
609   F. (2018a). Fate of particulate copper and zinc isotopes at the Solimões-Negro river
610   confluence, Amazon Basin, Brazil. *Chemical Geology*, *489*, 1–15.
611   https://doi.org/10.1016/j.chemgeo.2018.05.004

612 Guinoiseau, D., Bouchez, J., Gélabert, A., Louvat, P., Moreira-Turcq, P., Filizola, N., & Benedetti, M.
613   F. (2018b). Fate of particulate copper and zinc isotopes at the Solimões-Negro river
614   confluence, Amazon Basin, Brazil. *Chemical Geology*, *489*, 1–15.
615   https://doi.org/10.1016/j.chemgeo.2018.05.004

616 Guinoiseau, D., Gélabert, A., Allard, T., Louvat, P., Moreira-Turcq, P., & Benedetti, M. F. (2017).
617   Zinc and copper behaviour at the soil-river interface: New insights by Zn and Cu isotopes in
618   the organic-rich Rio Negro basin. *Geochimica et Cosmochimica Acta*, *213*, 178–197.
619   https://doi.org/10.1016/j.gca.2017.06.030

620 Ilina, S. M., Viers, J., Lapitsky, S. A., Mialle, S., Mavromatis, V., Chmeleff, J., Brunet, P., Alekhin, Y.
621   V., Isnard, H., & Pokrovsky, O. S. (2013). Stable (Cu, Mg) and radiogenic (Sr, Nd) isotope
622   fractionation in colloids of boreal organic-rich waters. *Chemical Geology*, *342*, 63–75.
623   https://doi.org/10.1016/j.chemgeo.2013.01.019

624 Jalón-Rojas, I., Schmidt, S., Sottolichio, A., & Bertier, C. (2016). Tracking the turbidity maximum
625   zone in the Loire Estuary (France) based on a long-term, high-resolution and high-frequency
626   monitoring network. *Continental Shelf Research*, *117*, 1–11.
627   https://doi.org/10.1016/j.csr.2016.01.017

628 Jeong, H., Ra, K., & Choi, J. Y. (2021). Copper, Zinc and Lead Isotopic Delta Values and Isotope
629   Ratios of Various Geological and Biological Reference Materials. *Geostandards and*
630   *Geoanalytical Research*, *45*(3), 551–563. https://doi.org/10.1111/ggr.12379

631 John, S. G., & Conway, T. M. (2014). A role for scavenging in the marine biogeochemical cycling of
632   zinc and zinc isotopes. *Earth and Planetary Science Letters*, *394*, 159–167.
633   https://doi.org/10.1016/j.epsl.2014.02.053

634 John, S. G., Geis, R. W., Saito, M. A., & Boyle, E. A. (2007). Zinc isotope fractionation during high-
635   affinity and low-affinity zinc transport by the marine diatom *Thalassiosira oceanica*.
636   *Limnology and Oceanography*, *52*(6), 2710–2714. https://doi.org/10.4319/lo.2007.52.6.2710

637 John, S. G., Helgoe, J., & Townsend, E. (2018). Biogeochemical cycling of Zn and Cd and their stable
638   isotopes in the Eastern Tropical South Pacific. *Marine Chemistry*, *201*, 256–262.
639   https://doi.org/10.1016/j.marchem.2017.06.001

640 Köbberich, M., & Vance, D. (2018). Zinc association with surface-bound iron-hydroxides on cultured
641   marine diatoms: A zinc stable isotope perspective. *Marine Chemistry*, *202*, 1–11.
642   https://doi.org/10.1016/j.marchem.2018.01.002

643 Köbberich, M., & Vance, D. (2019). Zn isotope fractionation during uptake into marine
644   phytoplankton: Implications for oceanic zinc isotopes. *Chemical Geology*, *523*, 154–161.
645   https://doi.org/10.1016/j.chemgeo.2019.04.004

646 Komárek, M., Ratié, G., Vaňková, Z., Šípková, A., & Chrastný, V. (2021). Metal isotope
647   complexation with environmentally relevant surfaces: Opening the isotope fractionation black

648 box. *Critical Reviews in Environmental Science and Technology*, *0*(0), 1–31.
649 https://doi.org/10.1080/10643389.2021.1955601

650 Lam, P. J., Lee, J.-M., Heller, M. I., Mehic, S., Xiang, Y., & Bates, N. R. (2018). Size-fractionated
651 distributions of suspended particle concentration and major phase composition from the U.S.
652 GEOTRACES Eastern Pacific Zonal Transect (GP16). *Marine Chemistry*, *201*, 90–107.
653 https://doi.org/10.1016/j.marchem.2017.08.013

654 Lazure, P., Dumas, F., & Vrignaud, C. (2008). Circulation on the Armorican shelf (Bay of Biscay) in
655 autumn. *Journal of Marine Systems*, *72*(1), 218–237.
656 https://doi.org/10.1016/j.jmarsys.2007.09.011

657 Lazure, P., & Jegou, A.-M. (1998). 3D modelling of seasonal evolution of Loire and Gironde plumes
658 on Biscay Bay continental shelf. *Oceanologica Acta*, *21*(2), 165–177.
659 https://doi.org/10.1016/S0399-1784(98)80006-6

660 Li, D., & Liu, S.-A. (2022). Copper Isotope Fractionation during Basalt Leaching at 25 °C and pH =
661 0.3, 2. *Journal of Earth Science*, *33*(1), 82–91. https://doi.org/10.1007/s12583-021-1499-7

662 Li, D., Liu, S.-A., & Li, S. (2015). Copper isotope fractionation during adsorption onto kaolinite:
663 Experimental approach and applications. *Chemical Geology*, *396*, 74–82.
664 https://doi.org/10.1016/j.chemgeo.2014.12.020

665 Liang, L., Liu, C.-Q., Zhu, X., Ngwenya, B. T., Wang, Z., Song, L., & Li, J. (2020). Zinc Isotope
666 Characteristics in the Biogeochemical Cycle as Revealed by Analysis of Suspended
667 Particulate Matter (SPM) in Aha Lake and Hongfeng Lake, Guizhou, China. *Journal of Earth
668 Science*, *31*(1), 126–140. https://doi.org/10.1007/s12583-017-0957-8

669 Little, S. H., Archer, C., Milne, A., Schlosser, C., Achterberg, E. P., Lohan, M. C., & Vance, D.
670 (2018). Paired dissolved and particulate phase Cu isotope distributions in the South Atlantic.
671 *Chemical Geology*, *502*, 29–43. https://doi.org/10.1016/j.chemgeo.2018.07.022

672 Little, S. H., Vance, D., Walker-Brown, C., & Landing, W. M. (2014). The oceanic mass balance of
673 copper and zinc isotopes, investigated by analysis of their inputs, and outputs to
674 ferromanganese oxide sediments. *Geochimica et Cosmochimica Acta*, *125*, 673–693.
675 https://doi.org/10.1016/j.gca.2013.07.046

676 Ma, L., Li, Y., Wang, W., Weng, N., Evans, R. D., & Wang, W.-X. (2019). Zn Isotope Fractionation
677 in the Oyster *Crassostrea hongkongensis* and Implications for Contaminant Source Tracking.
678 *Environmental Science & Technology*, *53*(11), 6402–6409.
679 https://doi.org/10.1021/acs.est.8b06855

680 Ma, L., Wang, W., Xie, M.-W., Wang, W.-X., & Evans, R. D. (2020). Using Zn Isotopic Signatures
681 for Source Identification in a Contaminated Estuary of Southern China. *Environmental
682 Science & Technology*, *54*(8), 5140–5149. https://doi.org/10.1021/acs.est.9b05955

683 Ma, L., & Wang, W.-X. (2021). Zinc source differentiation in hydrothermal vent mollusks: Insight
684 from Zn isotope ratios. *Science of The Total Environment*, *773*, 145653.
685 https://doi.org/10.1016/j.scitotenv.2021.145653

686 Ma, L., Wang, W.-X., & Evans, R. D. (2021). Distinguishing multiple Zn sources in oysters in a
687 complex estuarine system using Zn isotope ratio signatures. *Environmental Pollution*, *289*,
688 117941. https://doi.org/10.1016/j.envpol.2021.117941

689 Mason, R. P. (2013). *Trace Metals in Aquatic Systems: Mason/Trace Metals in Aquatic Systems*. John
690 Wiley & Sons, Ltd. https://doi.org/10.1002/9781118274576

691 Meglen, R. R. (1992). Examining large databases: A chemometric approach using principal
692 component analysis. *Marine Chemistry*, *39*(1–3), 217–237. https://doi.org/10.1016/0304-
693 4203(92)90103-H

694 Morel, F. M. M. (2003). The Biogeochemical Cycles of Trace Metals in the Oceans. *Science*,
695 *300*(5621), 944–947. https://doi.org/10.1126/science.1083545

696 Moynier, F., Vance, D., Fujii, T., & Savage, P. (2017). The Isotope Geochemistry of Zinc and Copper.
697 *Reviews in Mineralogy and Geochemistry*, *82*(1), 543–600.
698 https://doi.org/10.2138/rmg.2017.82.13

699 Nitzsche, K. N., Yoshimura, T., Ishikawa, N. F., Ogawa, N. O., Suzuki, K., & Ohkouchi, N. (2021).
700 Trace metal geochemical and Zn stable isotope data as tracers for anthropogenic metal
701 contributions in a sediment core from Lake Biwa, Japan. *Applied Geochemistry*, *134*, 105107.
702 https://doi.org/10.1016/j.apgeochem.2021.105107

703 Peel, K., Weiss, D., & Siggc, L. (2009). Zinc isotope composition of settling particles as a proxy for
704   biogeochemical processes in lakes: Insights from the eutrophic Lake Greifen, Switzerland.
705   *Limnology and Oceanography*, *54*(5), 1699–1708. https://doi.org/10.4319/lo.2009.54.5.1699

706 Penaud, A., Ganne, A., Eynaud, F., Lambert, C., Coste, P. O., Herlédan, M., Vidal, M., Goslin, J.,
707   Stéphan, P., Charria, G., Pailler, Y., Durand, M., Zumaque, J., & Mojtahid, M. (2020).
708   Oceanic versus continental influences over the last 7 kyrs from a mid-shelf record in the
709   northern Bay of Biscay (NE Atlantic). *Quaternary Science Reviews*, *229*, 106135.
710   https://doi.org/10.1016/j.quascirev.2019.106135

711 Petit, J. C. J., Schäfer, J., Coynel, A., Blanc, G., Chiffoleau, J.-F., Auger, D., Bossy, C., Derriennic,
712   H., Mikolaczyk, M., Dutruch, L., & Mattielli, N. (2015). The estuarine geochemical reactivity
713   of Zn isotopes and its relevance for the biomonitoring of anthropogenic Zn and Cd
714   contaminations from metallurgical activities: Example of the Gironde fluvial-estuarine system,
715   France. *Geochimica et Cosmochimica Acta*, *170*, 108–125.
716   https://doi.org/10.1016/j.gca.2015.08.004

717 Petit, J. C. J., Schäfer, J., Coynel, A., Blanc, G., Deycard, V. N., Derriennic, H., Lanceleur, L.,
718   Dutruch, L., Bossy, C., & Mattielli, N. (2013). Anthropogenic sources and biogeochemical
719   reactivity of particulate and dissolved Cu isotopes in the turbidity gradient of the Garonne
720   River (France). *Chemical Geology*, *359*, 125–135.
721   https://doi.org/10.1016/j.chemgeo.2013.09.019

722 Rao, C. R. M., Sahuquillo, A., & Lopez Sanchez, J. F. (2008). A Review of the Different Methods
723   Applied in Environmental Geochemistry For Single and Sequential Extraction of Trace
724   Elements in Soils and Related Materials. *Water, Air, and Soil Pollution*, *189*(1), 291–333.
725   https://doi.org/10.1007/s11270-007-9564-0

726 Schleicher, N. J., Dong, S., Packman, H., Little, S. H., Ochoa Gonzalez, R., Najorka, J., Sun, Y., &
727   Weiss, D. J. (2020). A Global Assessment of Copper, Zinc, and Lead Isotopes in Mineral Dust
728   Sources and Aerosols. *Frontiers in Earth Science*, *8*. https://doi.org/10.3389/feart.2020.00167

729 Schulz, H. D., & Zabel, M. (Eds.). (2006). *Marine Geochemistry*. Springer-Verlag.
730   https://doi.org/10.1007/3-540-32144-6

731 Sherman, D. M., & Little, S. H. (2020). Isotopic disequilibrium of Cu in marine ferromanganese
732   crusts: Evidence from ab initio predictions of Cu isotope fractionation on sorption to
733   birnessite. *Earth and Planetary Science Letters*, *549*, 116540.
734   https://doi.org/10.1016/j.epsl.2020.116540

735 Skierszkan, E. K., Mayer, K. U., Weis, D., & Beckie, R. D. (2016). Molybdenum and zinc stable
736   isotope variation in mining waste rock drainage and waste rock at the Antamina mine, Peru.
737   *Science of The Total Environment*, *550*, 103–113.
738   https://doi.org/10.1016/j.scitotenv.2016.01.053

739 Souto-Oliveira, C. E., Babinski, M., Araújo, D. F., Weiss, D. J., & Ruiz, I. R. (2019). Multi-isotope
740   approach of Pb, Cu and Zn in urban aerosols and anthropogenic sources improves tracing of
741   the atmospheric pollutant sources in megacities. *Atmospheric Environment*, *198*, 427–437.
742   https://doi.org/10.1016/j.atmosenv.2018.11.007

743 Sparks, D. L. (2005). Toxic Metals in the Environment: The Role of Surfaces. *Elements*, *1*(4), 193–
744   197. https://doi.org/10.2113/gselements.1.4.193

745 Strady, E., Harmelin-Vivien, M., Chiffoleau, J. F., Veron, A., Tronczynski, J., & Radakovitch, O.
746   (2015). 210Po and 210Pb trophic transfer within the phytoplankton–zooplankton–
747   anchovy/sardine food web: A case study from the Gulf of Lion (NW Mediterranean Sea).
748   *Journal of Environmental Radioactivity*, *143*, 141–151.
749   https://doi.org/10.1016/j.jenvrad.2015.02.019

750 Suhr, N., Schoenberg, R., Chew, D., Rosca, C., Widdowson, M., & Kamber, B. S. (2018). Elemental
751   and isotopic behaviour of Zn in Deccan basalt weathering profiles: Chemical weathering from
752   bedrock to laterite and links to Zn deficiency in tropical soils. *Science of The Total
753   Environment*, *619–620*, 1451–1463. https://doi.org/10.1016/j.scitotenv.2017.11.112

754 Takano, S., Liao, W.-H., Tian, H.-A., Huang, K.-F., Ho, T.-Y., & Sohrin, Y. (2020). Sources of
755   particulate Ni and Cu in the water column of the northern South China Sea: Evidence from
756   elemental and isotope ratios in aerosols and sinking particles. *Marine Chemistry*, *219*, 103751.
757   https://doi.org/10.1016/j.marchem.2020.103751

758 Tessier, A., & Turner, D. R. (Eds.). (1995). *Metal speciation and bioavailability in aquatic systems*. J.
759   Wiley.

760 Thapalia, A., Borrok, D. M., Van Metre, P. C., & Wilson, J. (2015). Zinc Isotopic Signatures in Eight
761   Lake Sediment Cores from Across the United States. *Environmental Science & Technology*,
762   *49*(1), 132–140. https://doi.org/10.1021/es5036893

763 Tonhá, M. S., Araújo, D. F., Araújo, R., Cunha, B. C. A., Machado, W., Portela, J. F., PR Souza, J.,
764   Carvalho, H. K., Dantas, E. L., Roig, H. L., Seyler, P., & Garnier, J. (2021). Trace metal
765   dynamics in an industrialized Brazilian river: A combined application of Zn isotopes,
766   geochemical partitioning, and multivariate statistics. *Journal of Environmental Sciences*, *101*,
767   313–325. https://doi.org/10.1016/j.jes.2020.08.027

768 Tonhá, M. S., Garnier, J., Araújo, D. F., Cunha, B. C. A., Machado, W., Dantas, E., Araújo, R., Kutter,
769   V. T., Bonnet, M.-P., & Seyler, P. (2020). Behavior of metallurgical zinc contamination in
770   coastal environments: A survey of Zn from electroplating wastes and partitioning in
771   sediments. *Science of The Total Environment*, 140610.
772   https://doi.org/10.1016/j.scitotenv.2020.140610

773 Turner, A., & Millward, G. E. (2002). Suspended Particles: Their Role in Estuarine Biogeochemical
774   Cycles. *Estuarine, Coastal and Shelf Science*, *55*(6), 857–883.
775   https://doi.org/10.1006/ecss.2002.1033

776 Twining, B. S., & Baines, S. B. (2013). The Trace Metal Composition of Marine Phytoplankton.
777   *Annual Review of Marine Science*, *5*(1), 191–215. https://doi.org/10.1146/annurev-marine-
778   121211-172322

779 Unda-Calvo, J., Ruiz-Romera, E., Fdez-Ortiz de Vallejuelo, S., Martínez-Santos, M., & Gredilla, A.
780   (2019). Evaluating the role of particle size on urban environmental geochemistry of metals in
781   surface sediments. *Science of The Total Environment*, *646*, 121–133.
782   https://doi.org/10.1016/j.scitotenv.2018.07.172

783 Vance, D., Matthews, A., Keech, A., Archer, C., Hudson, G., Pett-Ridge, J., & Chadwick, O. A.
784   (2016). The behaviour of Cu and Zn isotopes during soil development: Controls on the
785   dissolved load of rivers. *Chemical Geology*. https://doi.org/10.1016/j.chemgeo.2016.06.002

786 Viers, J., Grande, J. A., Zouiten, C., Freydier, R., Masbou, J., Valente, T., Torre, M.-L. de la,
787   Destrigneville, C., & Pokrovsky, O. S. (2018). Are Cu isotopes a useful tool to trace metal
788   sources and processes in acid mine drainage (AMD) context? *Chemosphere*, *193*, 1071–1079.
789   https://doi.org/10.1016/j.chemosphere.2017.11.133

790 von der Heyden, B. P., & Roychoudhury, A. N. (2015). Application, Chemical Interaction and Fate of
791   Iron Minerals in Polluted Sediment and Soils. *Current Pollution Reports*, *1*(4), 265–279.
792   https://doi.org/10.1007/s40726-015-0020-2

793 Weber, T., John, S., Tagliabue, A., & DeVries, T. (2018). Biological uptake and reversible scavenging
794   of zinc in the global ocean. *Science*, *361*(6397), 72–76.
795   https://doi.org/10.1126/science.aap8532

796 Weiss, D. J., Rausch, N., Mason, T. F. D., Coles, B. J., Wilkinson, J. J., Ukonmaanaho, L., Arnold, T.,
797   & Nieminen, T. M. (2007). Atmospheric deposition and isotope biogeochemistry of zinc in
798   ombrotrophic peat. *Geochimica et Cosmochimica Acta*, *71*(14), 3498–3517.
799   https://doi.org/10.1016/j.gca.2007.04.026

800 Wiederhold, J. G. (2015). Metal Stable Isotope Signatures as Tracers in Environmental Geochemistry.
801   *Environmental Science & Technology*, *49*(5), 2606–2624. https://doi.org/10.1021/es504683e

802 Yang, S.-C., Hawco, N. J., Pinedo-Gonzalez, P., Bian, X., Huang, K.-F., Zhang, R., & John, S. G.
803   (2020). A new purification method for Ni and Cu stable isotopes in seawater provides
804   evidence for widespread Ni isotope fractionation by phytoplankton in the North Pacific.
805   *Chemical Geology*, *547*, 119662. https://doi.org/10.1016/j.chemgeo.2020.119662

806 Zhang, R., Russell, J., Xiao, X., Zhang, F., Li, T., Liu, Z., Guan, M., Han, Q., Shen, L., & Shu, Y.
807   (2018). Historical records, distributions and sources of mercury and zinc in sediments of East
808   China sea: Implication from stable isotopic compositions. *Chemosphere*, *205*, 698–708.
809   https://doi.org/10.1016/j.chemosphere.2018.04.100

810 Zhang, Y., Planavsky, N. J., Zhao, M., Isson, T., Asael, D., Wang, C., & Wang, F. (2021). The
811   isotopic composition of sedimentary organic zinc and implications for the global Zn isotope
812   mass balance. *Geochimica et Cosmochimica Acta*, *314*, 16–26.
813   https://doi.org/10.1016/j.gca.2021.09.009
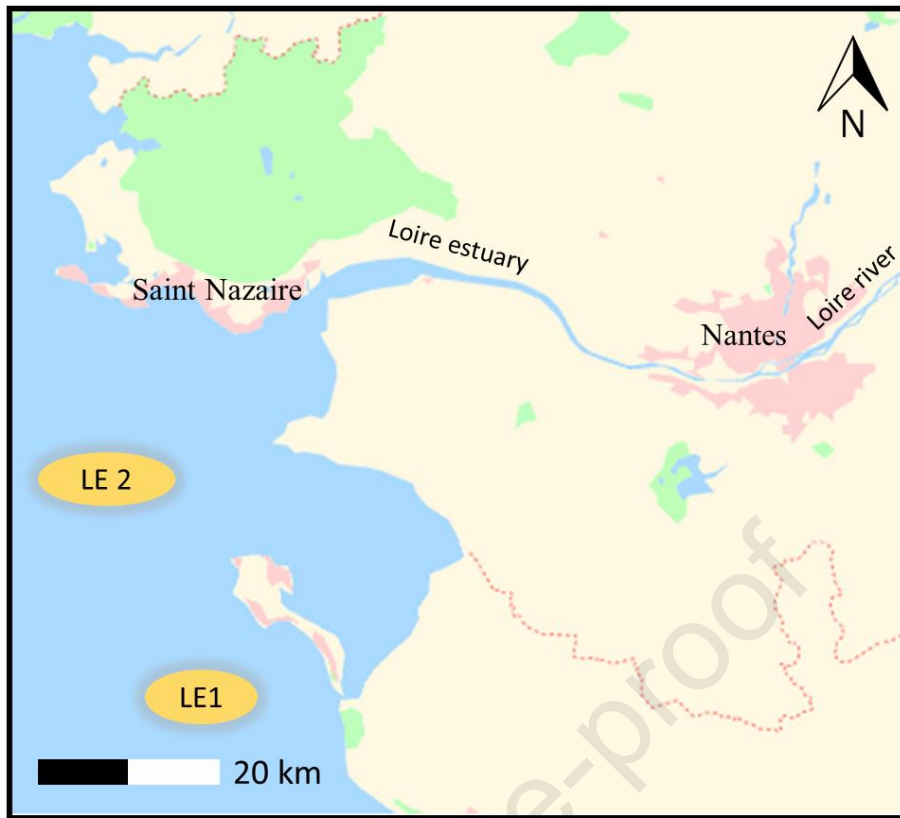
814

815 **Fig. 1** Sampling stations (LE1 and LE2) for suspended particulate matter in the Northern Bay of Biscay.

816
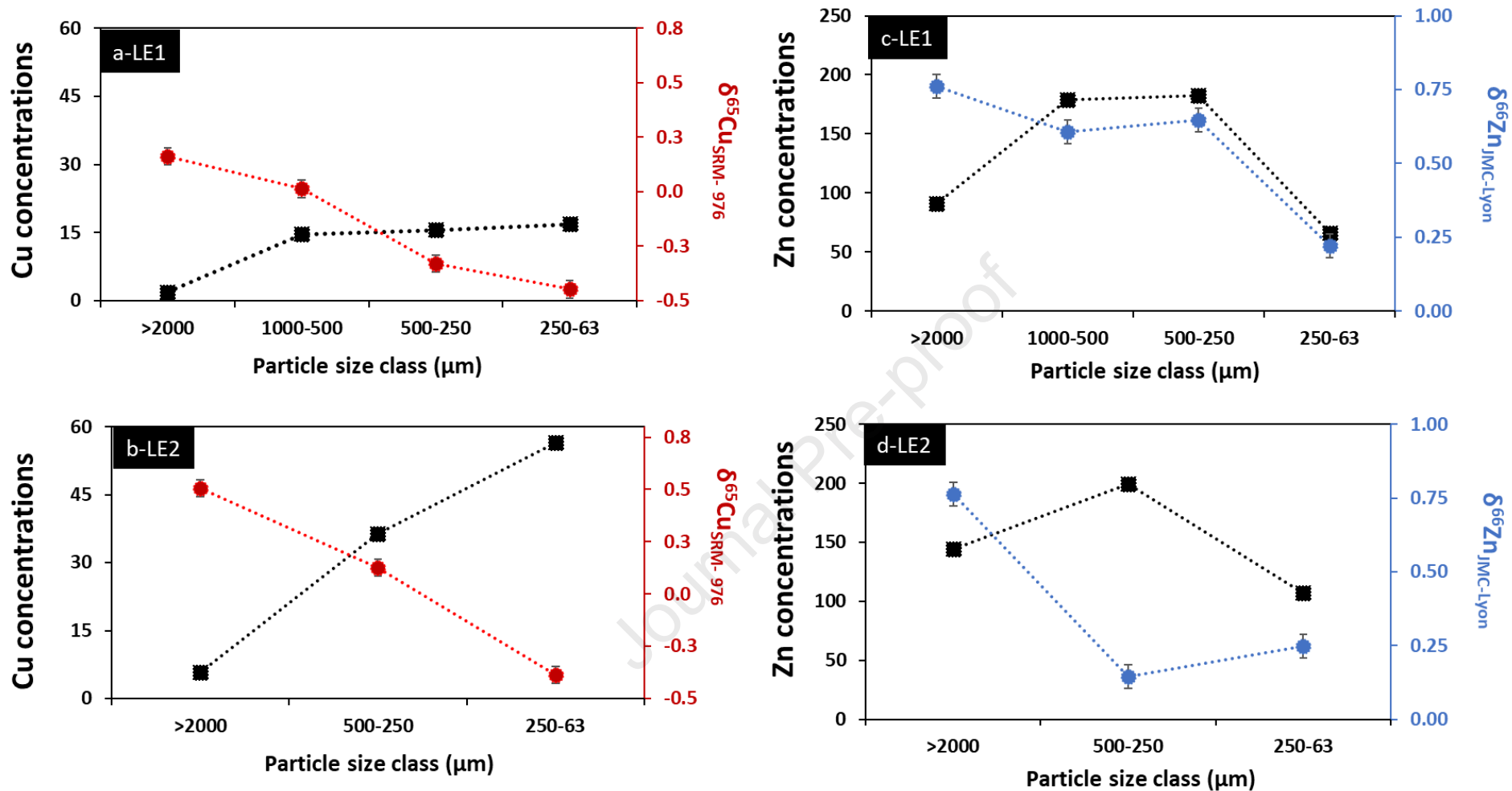
Fig. 2 Concentrations (µg g^{-1}, dry weight) and isotope compositions of Cu and Zn (in per mil, ‰) in SPM sub-fractions collected at the LE1 and LE2 sampling stations. Sub-fractions comprise the different particle size classes of SPM (µm): >2000; 1000-500; 500-250; 250-63. The fraction 1000-5000 µm is missing for LE2 due lack of sufficient material for analyses.
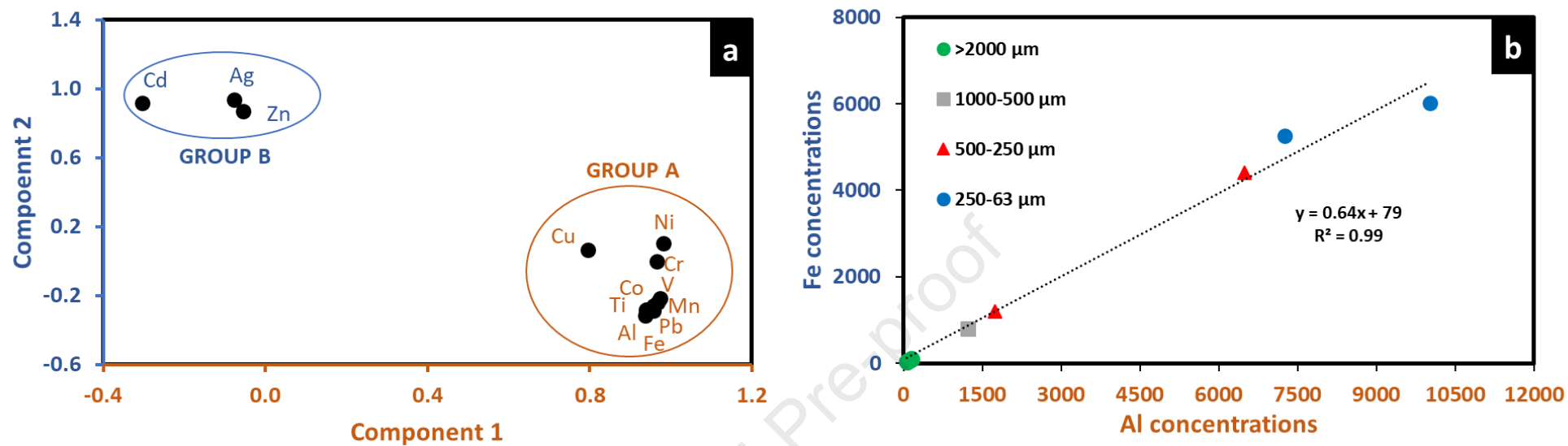
Fig. 3 (a) Principal component analysis for trace and major elemental dataset of SPM and the identification of intercorrelated elements in clusters: Group A and Group B, respectively; **(b)** regression analysis for Fe and Al concentrations (μg g^{-1}, dry weight).
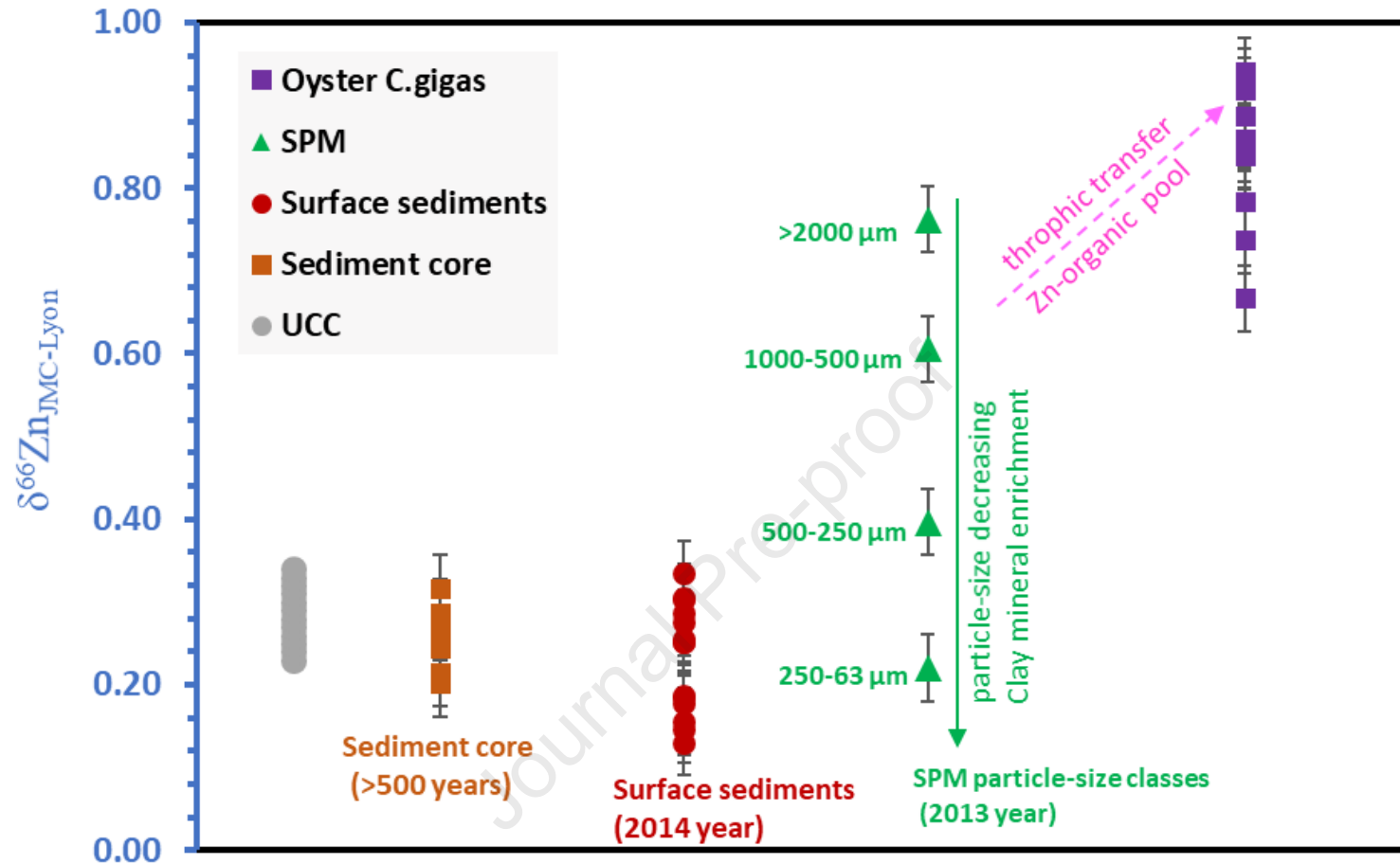
Fig.4 Zn multi-compartmental isotope variability in the Loire estuary and Upper Continental Crust (UCC). δ^{66}Zn value average of SPM particle-size fractions (this study) is compared to sediments (Araújo et al., 2019b) and primary consumers (oysters, Araújo, et al., 2021) reported in previous studies. A sediment core ("PV1") integrate an isotope record of at least 500 years. Zinc isotope range of the UCC is reported by (Moynier et al., 2017). Clay mineral may be coated by Fe and Al oxides and biofilms. As clay minerals contents decrease with particle-size increasing, Zn organic pool becomes prevalent, and the SPM δ^{66}Zn value shifts up. This tendency implies that the Zn-organic pool present in the different SPM fractions presents heavier isotope compositions. Therefore, the high δ^{66}Zn values of oyster's soft tissues are consistent with the hypothesis of bioaccumulation of a local available Zn-organic pool enriched in the heavy Zn isotope.

Table 1. Elemental concentrations (µg g⁻¹, dry weight) and Cu and Zn isotope compositions (‰) dataset for different particle-size fractions of SPM from the Loire estuary mouth. δ-values for Cu and Zn are calculated in relation to the reference materials "NIST-SRM 976" and "JMC-Lyon", respectively. Isotope data for reference materials (RMs) represent the average of replicates, this is, distinct aliquots processed through digestion, chromatography and measured twice or thrice by MC-ICP-MS.

Sample	δ^{65}Cu	2s	δ^{66}Zn	2s	Cu	Zn	Fe	Al	Ti	V	Cr	Mn	Co	Ni	Ag	Cd	Pb
LE1 63-250 µm	-0.45	0.01	0.22	0.01	17	66	6023	10016	233	17.2	13.7	84	1.94	7.0	0.04	0.08	6.9
LE1 250-500 µm	-0.33	0.02	0.65	0.03	16	183	1202	1734	62	3.7	6.1	22	0.52	4.1	0.19	0.48	1.5
LE1 500-1000 µm	0.01	0.06	0.61	0.02	15	179	801	1226	46	2.8	6.7	16	0.38	4.3	0.16	0.45	1.1
LE1 >2000 µm	0.16	0.06	0.76	0.07	2	91	39	63	19	0.2	2.1	1	0.05	1.1	0.04	0.14	0.1
LE2 63-250 µm	-0.39	0.01	0.25	0.00	57	107	5267	7254	162	12.1	15.1	70	1.61	6.8	0.05	0.13	7.5
LE2 250-500 µm	0.12	0.01	0.14	0.02	36	200	4406	6489	161	10.8	18.3	68	1.40	6.5	0.07	0.17	5.5
LE2 >2000 µm	0.51	0.01	0.76	0.04	6	144	93	141	20	0.3	1.0	2	0.05	0.5	0.04	0.21	0.1
Reference Materials																	
BCR 414	-0.27 *n* = 3	0.02	0.23 *n* = 1	0.09													
SRM 1566b	0.23 *n* = 11	0.03	0.70 *n* = 5	0.05													
MESS-3	0.03 *n* = 10	0.08	0.26 *n* = 10	0.06													

Highlights

- Cu and Zn isotopes in different particle sizes of SPM from Biscay Bay.

- Four size fractions (63-250; 250-500; 500-1000; and >2000 µm) were target.

- Isotopes help identify geogenic and bioavailable pools in SPM sub-fractions.

- Geogenic pools are enriched in the light and bioavailable pools in the heavy isotopes.

- Isotopes in SPM sub-fractions may help to constrain food-web metal transfers.

Research paper

Cu and Zn stable isotopes in suspended particulate matter sub-fractions from the Northern Bay of Biscay help identify biogenic and geogenic particle pools

Daniel F. Araújo[a]*, Joël Knoery[a], Nicolas Briant[a], Emmanuel Ponzevera[a], Daniel Santos Mulholland[b] Sandrine Bruzac[a], Teddy Sireau[a], Tiphaine Chouvelon[a-c], Christophe Brach-Papa[d]

a. Ifremer, CCEM Centre Atlantique, Unité Contamination Chimique des Écosystèmes Marins, F-44000 Nantes, France
b. Laboratório de Águas e Efluentes & Laboratório de Análises Ambientais, Universidade Federal do Tocantins, Rua Badejos, Gurupi, TO – Brasil
c. Observatoire Pelagis, UAR 3462 La Rochelle Université-CNRS, 17000 La Rochelle, France
d. Ifremer, Centre Méditerranée, Unité Littoral, Laboratoire Environnement Ressources Provence-Azur-Corse (LERPAC), 83507, La Seyne-sur-Mer Cedex, France